AAV-mediated gene therapy in a GLDC-deficient mouse model of Non-Ketotic Hyperglycinemia

Kit-Yi Leung[1], Chloe Santos[1], Sandra C.P. De Castro[1], Diana Gold Diaz[1], Andrew J. Copp[1], Simon Waddington[2], Nicholas DE Greene[1]*

[1] Developmental Biology and Cancer Department, Great Ormond Street Institute of Child Health, University College London, London, UK

[2] EGA Institute for Women's Health, University College London, London, UK

*Correspondence: NDE Greene, Developmental Biology & Cancer Department, UCL Great Ormond Street Institute of Child Health, 30 Guilford Street, London, WC1N 1EH, UK.

n.greene@ucl.ac.uk Tel: +44 2079052217 orcid.org/0000-0002-4170-5248

Abstract

Non-Ketotic Hyperglycinemia is a rare inborn error of metabolism caused by impaired function of the glycine cleavage system (GCS) and characterised by accumulation of glycine in body fluids and tissues. Severe NKH presents in neonates with hypotonia, apnea and seizures and affected infants display profound developmental delay and complex epilepsy. NKH is an autosomal recessive condition, and the majority of affected individuals carry mutations in *GLDC* (glycine decarboxylase). Current treatments for NKH are not effective or curative. NKH is inherited as a monogenic condition with known genetic causation and is therefore potentially amenable to gene therapy. An AAV9-based gene therapy vector was designed to target sites of GCS activity in liver and brain. Using a ubiquitous promoter to drive expression of a GFP reporter, administration of vector at neonatal stages by intra-venous and/or intra-cerebroventricular route was confirmed to result in transduction of both liver and brain. Using the same capsid and promoter with transgenes to express mouse or human GLDC, vectors were then tested in a GLDC-deficient mouse model, that recapitulates key features of NKH including elevated plasma glycine concentration, accumulation of glycine in liver and brain tissues, and suppression of folate one-carbon metabolism and related metabolites. Neonatal administration of vector achieved reinstatement of *GLDC* mRNA and protein expression in GLDC-deficient mice. Treated GLDC-deficient mice showed significant lowering of plasma glycine, confirming functionality of vector expressed protein. AAV9-GLDC treatment also led to lowering of brain tissue glycine, and normalisation of the folate profile indicating restoration of glycine-derived one-carbon supply. These findings support the hypothesis that AAV-mediated gene therapy may offer potential in treatment of NKH.

Introduction

Non-Ketotic Hyperglycinemia (NKH; glycine encephalopathy) is a life-limiting autosomal recessive disease, characterised by accumulation of glycine in body fluids and tissues [1-3]. Severe NKH presents in neonates, with lethargy, respiratory problems (apnea) that may require assisted breathing, hypotonia and seizures. Myoclonic jerks and burst suppression pattern on EEG are frequently present in neonates but the type, frequency and severity of seizures changes in infants, to include hypsarrhythmia, burst suppression and multifocal epilepsy [4]. This clinical course highlights opportunity for early therapy that could prevent secondary epilepsy-related neurological damage. Surviving infants suffer profound neurological impairment with complex epilepsy and profound psychomotor retardation [1,5]. Around one-third of affected individuals die within the first year and the median age of death is 8 years.

NKH is caused by loss of function of the glycine cleavage system (GCS), an evolutionarily conserved mitochondrial protein complex that acts to decarboxylate glycine with concomitant transfer of a one-carbon group to tetrahydrofolate (THF) in folate one-carbon metabolism (FOCM)[2,6] . The GCS has four protein components, of which glycine decarboxylase (GLDC) and aminomethyltransferase (AMT) are thought to be GCS-specific, whereas GCS H protein (GSCH) and dihydrolipoamide dehydrogenase (DLD) have additional roles in other enzyme complexes [7,8]. Approximately 80% of individuals with NKH carry mutations in *GLDC* with majority of the other cases being attributable to mutations in *AMT* [6,9], and a small number to *GCSH* [10]. In a subset of cases, described as 'variant NKH' mutations in GCS-encoding genes are not detected and, in some individuals, mutations have been identified in the enzyme pathway responsible for synthesis of the lipoate co-factor, which is responsible for lipoylation of GCSH and other proteins [11,12].

In addition to severe NKH that presents in neonates or infants, it has become evident that a wider spectrum of disease is associated with GCS mutations. Attenuated NKH appears to result from *GLDC* or *AMT* mutations that result in partial loss of protein function, with heterogeneity in age of onset and a less severe neurological outcome [5], but still a debilitating disease. Identification of *GLDC* mutations in children or adults with mental retardation and behavioural problems [13-15], further suggests that mild or late-onset NKH may go unrecognised

in some individuals.

Current treatment for NKH is largely focussed on control of glycine and amelioration of the predicted epileptogenic effects of glycine. Administration of sodium benzoate can lower glycine levels via stimulation of the glycine conjugation pathway in liver and kidneys, resulting on production of benzoylglycine (hippurate) that is excreted in urine [16,17]. In addition, multiple anti-epileptics and the NMDA-receptor antagonist dextromethorphan are frequently used in order to mitigate the effects of excess glycine in the brain [18-20]. These treatments are not curative, and do not appreciably improve neurodevelopment, while benzoate treatment has associated side-effects and requires co-administration of antacids [17,21].

While current treatments for NKH are not effective, the continuum of clinical severity from neonatal onset, severe NKH to milder and later-onset forms suggests that therapies which reinstate GCS function may have a beneficial effect. Unlike current treatments, restoration of GCS function would achieve both lowering of glycine and supply of glycine-derived one-carbon groups to FOCM. Gene therapy vectors provide potential to deliver a *GLDC* transgene to endogenous sites of expression in the liver and brain, and this approach would potentially be applicable to any loss of function mutation in *GLDC*.

Adeno-associated virus (AAV) based vectors are based on the AAV genome with replacement of the *rep* and *cap* genes by the therapeutic transgene and promoter. AAV vectors enter the target cell nucleus and exist primarily in episomal form with rare integration into the host chromosomes. Hence, long-term expression of transgenes may be achieved in non-dividing cells, such as neurons, although the vector may be 'diluted' in tissues undergoing cell proliferation [22,23]. The cell-type specificity (tropism) of AAV is determined by the capsid varies with serotype, Tissue specificity of AAV transduction has been found to be effective in crossing the blood brain barrier and can transduce neurons and non-neuronal cells, including astrocytes [22,24]. AAV9-based vectors have been used effectively in mouse models of several monogenic diseases including Krabbe disease, Niemann Pick type C and amyotrophic lateral sclerosis [25-30]. Successful testing of AAV9 vectors in animal model led to their implementation for clinical applications, for example, in treatment of spinal muscular atrophy [31-33].

As a model for testing potential novel treatments, mice that are homozygous for a gene-trap allele of *Gldc* (*Gldc*^{GT1}) provide a GLDC-deficient model for NKH [34]. *Gldc*$^{GT1/GT1}$ mice exhibit 90% reduction in *Gldc* mRNA abundance, undetectable GCS activity and hallmark features of NKH, including elevated glycine concentrations in blood, urine and tissues [34]. In addition to glycine, GLDC-deficient mice display tissue-dependent accumulation of multiple glycine derivatives including acylglycines and guanidinoacetate, which is reversible by liver-specific rescue of *Gldc* expression [34,35]. In accordance with predicted effects of GCS loss of function [2], GLDC-deficient mice exhibit suppression of folate one-carbon metabolism, with accumulation of tetrahydrofolate (THF) at the expense of folates that carry one-carbon groups [34,36]. In the current study we made use of the GLDC-deficient mouse model to test AAV9 vectors, owing to their ability to transduce liver and brain, the key target tissues in NKH.

Results

Among tissues in mammals and birds, GCS activity is highest in liver, kidney and brain, correlating with localisation of *GLDC* mRNA [2,37]. Liver activity of the GCS is sufficient to regulate circulating glycine levels in a non-tissue autonomous manner in mice [35]. However, GCS-mediated supply of glycine-derived one-carbon units in mitochondrial FOCM is predicted to be tissue autonomous. We therefore aimed to target liver and/or brain for AAV-mediated reinstatement of *Gldc* expression. The AAV9 capsid was selected based reported transduction of hepatocytes and CNS following administration to neonatal mice [38-40].

Although some studies have reported that vector genomes of up to 6 kb or even greater can be packaged in AAV vectors, the capacity is typically considered to be up to approximately 5 kb, corresponding to the size of the parental genome [41,42]. To drive broad expression in transduced tissues and to circumvent packaging limitations we designed a vector using AAV2 ITRs, hybrid chicken beta-actin (CBh) promoter and the GLDC-expressing transgene.

Transduction of brain and liver following neonatal administration of AAV9 vector

To assess transduction of target tissues and activity of the CBh promoter we performed preliminary studies using an eGFP transgene, packaged as AAV9-CBh-eGFP (Figure 1A). Vector was administered to wild-type (C57Bl/6) neonatal mice at post-natal day 1 (P1) by intravenous (iv) injection into the facial (temporal) vein, intracerebroventricular (ic) injection into the

lateral ventricle, or by both iv and ic (iv + ic) route. A further group of mice were administered vector at P20 via iv injection into the tail vein. Mice were sacrificed 3 weeks after vector administration for analysis of GFP mRNA and protein expression.

Expression of GFP mRNA was detected in both liver and brain, with varying abundance dependent on route and stage of administration. At 3 weeks post-treatment, expression in liver was higher in mice that were treated via iv or iv + ic routes at P1 compared with ic only, while expression following iv administration treatment at P20 was minimal compared with treatment at P1 (Figure 1B). Brain tissue was divided into anterior (olfactory bulbs and cortex) and posterior (mid and hindbrain) samples for mRNA quantification. Abundant GFP mRNA expression was detected in both regions following ic administration (with or without iv co-administration), while minimal mRNA was detected in brain following iv administration at P1 or P20 (Figure 1C).

At 3 weeks following neonatal injection (iv + ic route), immunostaining revealed presence of GFP protein in the liver and throughout the brain, including the cortex, hippocampus, and cerebellum (Figure 1D-G). Positive staining was detected in cells of differing morphology in cortex suggesting transduction and promoter activity in both neurons and astrocytes.

AAV vector containing a mouse *Gldc* transgene reinstates mRNA and protein expression in GLDC-deficient mice

The AAV vector with CBh promoter was modified to contain the mouse *Gldc* (mGLDC) coding sequence encoding the consensus wild-type GLDC protein, and packaged into AAV9 capsid. AAV9-CBh-mGLDC vector was administered to neonatal $Gldc^{GT1/GT1}$ mice by ic or iv + ic route. In the brain and liver of mice at 6 weeks post-administration, *Gldc* expression was analysed by quantitative real time RT-PCR (qRT-PCR). *Gldc* mRNA was significantly more abundant in vector-treated mice than in vehicle-treated $Gldc^{GT1/GT1}$ mice (Figure 2A-B), with approximately 50-fold and 15-fold increase in expression in brain and liver, respectively. Expression of *Gldc* in treated $Gldc^{GT1/Gt1}$ mice typically exceeded endogenous wild-type levels in the brain (Figure 2A) and varied from 50-100% of wild-type levels in the liver (Figure 2B).

Immunostaining for GLDC protein was used to confirm translation of the vector-expressed *Gldc* and assess distribution in the brain (Fig. 2C-H). Unlike in control *Gldc*$^{GT1/GT1}$ mice, where GLDC protein was virtually undetectable, vector treated *Gldc*$^{GT1/GT1}$ mice showed widespread expression in of GLDC in the brain, including in hippocampus, cortex and cerebellum (Figure 2F-H). GLDC staining in vector-treated mice was of similar intensity to wild-type mice in hippocampus and cerebellum, and even appeared more intense in the cortex. Hence, vector-mediated *Gldc* expression results in restoration of GLDC protein in the brain of treated mice, for at least 6 weeks after administration.

Normalisation of metabolic biomarkers in *Gldc*-deficient mice treated with AAV9-CBh-mGldc

Elevated plasma glycine, the hallmark biochemical biomarker of NKH is recapitulated in the *Gldc*-deficient mouse model, and can be normalised by conditional *Gldc* expression in the liver [35]. At 6 weeks of age, plasma glycine concentration was significantly higher in *Gldc*$^{GT1/GT1}$ mice than +/+ littermates (Figure 3A), with a non-significant trend towards higher glycine in females than males among *Gldc*$^{GT1/GT1}$ mice at this stage. Among mice treated neonatally with iv AAV9-CBh-mGLDC, leads to *Gldc* expression in liver, we observed significantly lower plasma glycine concentration than in untreated *Gldc*$^{GT1/GT1}$ mice (Figure 3A). As plasma glycine is regulated by liver GCS activity, this provides a measure of GLDC functionality. The treatment effect was observed in the overall cohort of mice and within male and female sub-groups. We conclude that vector expressed GLDC protein is functional and restores GCS activity.

As expected, we did not observe an effect on plasma glycine among mice in which *Gldc* expression was restored in brain but not liver, following vector administration by ic route only. However, we tested whether vector mediated GLDC expression in the brain was sufficient to lower tissue glycine content in *Gldc*$^{GT1/GT1}$ mice. We observed a significant reduction in brain tissue glycine content among mice at 6 weeks after neonatal treatment with AAV9-CBh-mGLDC by iv + ic or by ic route only (Figure 3B). It therefore appears that excess glycine in brain tissue can be removed by GCS activity within the brain, even when plasma glycine is not fully normalised.

In parallel with evaluating glycine control, we tested whether treatment affected the supply of one-carbon units into FOCM. As reported at embryonic stages [34], we found that the folate profile is abnormal in *Gldc*$^{GT1/GT1}$ brain tissue, with an increase in relative abundance of THF and decrease in abundance of 5-methyl THF (Figure 4A-B). Following treatment with AAV9-CBh-mGLDC at P1, the folate profile in brain tissue of *Gldc*$^{GT1/GT1}$ mice at 6 weeks was normalised, with the relative proportions of THF and 5-methyl THF showing no difference to wild-type tissue (Figure 4A-B). As a further read-out of FOCM function in brain tissue we analysed abundance of betaine and choline. Choline is the precursor of betaine, which in turn can act as a methyl donor in remethylation of homocysteine. We found that both metabolites are present at significantly lower levels in brain of *Gldc*$^{GT1/GT1}$ mice (Figure 4C-D). Concomitant with normalisation of the folate profile we observed restoration of betaine and choline abundance following AAV-mediated restoration of *Gldc* expression by neonatal iv + ic or ic routes of administration (Figure 4C-D).

Human GLDC is functional in mouse

Implementation of an AAV-based gene therapy for NKH will likely require a vector that leads to expression of the human GLDC protein. The GLDC protein in mouse (Uniprot Q91W43) and human (Uniprot P23378) comprise 1025 and 1020 amino acids respectively, with 92% identity. We hypothesised that the human protein would substitute for mouse GLDC in the GCS. Therefore, in order to test vectors expressing human GLDC we replaced the mouse *Gldc* coding sequence with a transgene sequence encoding the consensus human GLDC protein, and packaged this into AAV9 capsid. The AAV9-CBh-hGLDC vector was administered to neonatal *Gldc*$^{GT1/GT1}$ mice and tissues were collected for analysis at 6 weeks of age. Expression of *GLDC* was confirmed in liver and brain by qRT-PCR. GLDC protein expression was assessed by immunoblot and, as expected, endogenous mouse GLDC was detected in wild-type liver and brain but not in *Gldc*$^{GT1/GT1}$ mice (Figure 5A-B). In contrast, in samples from *Gldc*$^{GT1/GT1}$ mice that received neonatal treatment with AAV9-CBh-hGLDC, a GLDC band was present corresponding to vector-expressed GLDC. GLDC abundance in liver appeared to be lower than endogenous protein in liver but of greater abundance than endogenous protein in brain.

We further examined expression of human GLDC in the brain of treated *Gldc*-deficient mice by immunostaining of sagittal sections. Unlike in untreated *Gldc*$^{GT1/GT1}$ brain (Figure 5C), GLDC

staining was detected and appeared widespread in brain of AAV9-CBh-hGLDC treated *Gldc*$^{GT1/GT1}$ mice (Figure 5D-I), with intensity comparable to that of endogenous GLDC in untreated wild-type mice (Figure 5D-F).

Having confirmed that human GLDC is expressed in mice following AAV-vector administration we tested whether the human protein is functional in the context of the mouse GCS by analysis of plasma and brain tissue glycine (Figure 6). We observed significant lowering of plasma glycine at 6 weeks of age in vector-treated mice compared with untreated *Gldc*$^{GT1/GT1}$ mice (Figure 6A). In the brain of treated *Gldc*$^{GT1/GT1}$ the tissue glycine content was also significantly lowered compared to untreated *Gldc*-deficient mice, to a level that was comparable to wild-type (Figure 6B). Hence, vector expressed human GLDC is functional in the mouse.

Discussion

The GCS has two key functions, regulation of glycine concentration in tissues and supply of glycine-derived one carbon units to FOCM and downstream biochemical pathways. Disruption of each of these functions is thought to contribute to pathogenesis of NKH. As in humans, GCS disruption in mice leads to accumulation of glycine, and a series of glycine derivatives which may themselves be deleterious [34,35]. In parallel, impaired supply of one-carbon units leads to altered folate profile which we previously observed at embryonic stages and here confirmed in post-natal tissue. In addition to a shift in the folate profile, we found a reduced abundance of betaine and choline in the brain of *Gldc*-deficient mice which we hypothesise to reflect an increased requirement for betaine as a methyl donor owing to impaired supply of glycine-derived one-carbon groups via the GCS.

In the *Gldc*-deficient mouse model of NKH, treatment with benzoate or cinnamate is sufficient to lower circulating glycine [34,35], recapitulating the effect of benzoate in NKH patients [35]. However, this does not overcome suppression of FOCM and, as a therapeutic intervention in NKH, benzoate is associated with significant side effects including gastrointestinal irritation. Conversely, maternal supplementation of GLDC-deficient mice with formate, as a one-carbon donor, prevents the embryonic structural malformations that lead to neural tube defects and ventriculomegaly [34,35,43], but does not lower excess glycine [34].

The ability to reinstate GCS function through vector-mediated expression of a functional copy of the mutated protein in NKH (GLDC or AMT) would provide an opportunity to restore both glycine regulation and one-carbon metabolism. In the current study we tested this concept in the GLDC-deficient mouse model, and found that AAV-mediated expression of GLDC resulted in both lowering of plasma and tissue glycine, and normalisation of FOCM intermediates. Lowering of plasma glycine was achieved following iv administration of vector, with a lesser effect following ic administration, suggesting that this effect largely reflects GLDC expression in the liver, the major site of GCS activity. However, within the brain the tissue glycine content was normalised by ic (or ic + iv) treatment indicating that GCS activity within the brain may be sufficient to regulate glycine within this tissue (even if not normalised systemically). Similarly, FOCM-related metabolites were restored by vector administration to the brain. This treatment led to widespread expression of GFP reporter or GLDC, including sites of endogenous expression in hipocampus and cerebellum.

Expression of GLDC and normalisation of metabolite biomarkers in the brain was observed in young adult mice after neonatal administration, suggesting the potential for long-term benefit which will be evaluated in future studies. It was predicted that, as a predominantly non-integrating vector, AAV vector may become 'diluted' relative to total size of the liver owing to continuing cellular proliferation after neonatal administration of vector. However, significant lowering of plasma glycine, which reflects liver GCS activity, was still observed in young adults. Further studies will assess whether this effect persists longer-term. As a step towards long-term studies we found that neonatal administration of vector did not adversely affect survival or weight in wild-type mice maintained for up to 15 months.

Given that glycine conjugation and glycine cleavage are mediated by two separate enyzme systems, it is reasonable to predict that combined use of benzoate or cinnamate (to stimulate glycine conjugation [35]) with administration of GLDC-expressing AAV vector (to reinstate GCS) activity) could offer potential both for lowering plasma glycine and control of glycine with restoration of FOCM within the brain, or other target tissues.

Materials and Methods

Gldc-deficient mouse model of NKH

Anima studies were carried out under regulations of the Animals (Scientific Procedures) Act 1986 of the UK Government, and in accordance with the guidance issued by the Medical Research Council, UK in Responsibility in the Use of Animals for Medical Research (July 1993). *Gldc*-deficient mice ($Gldc^{GT1}$) carrying a gene-trap allele of *Gldc* were previously generated and characterised [34,35]. Mice used in the current study were on a C57BL/6J background. Experimental litters were generated by overnight timed mating of heterozygous ($Gldc^{GT1/+}$) male and female mice. Pregnant females were supplemented with formate in the drinking water (30 mg/ml) from day 7 top 14 of pregnancy to prevent neural tube defects among the offspring [34]. Mice were genotyped by PCR of genomic DNA [34].

AAV vectors

The AAV9-CBh-eGFP was obtained from Vector Biolabs (Malvern, PA, USA). GLDC cDNA sequences were synthesised (GenScript) and cloned into pAAV-ITR plasmid (containing AAV2 ITRs) downstream of a hybrid chicken beta-actin (CBh) promoter. Plasmids and vector were verified by sequencing to confirm encoding of wild-type protein (mouse NP_613061, human NP_000161). Vector production was performed by Vector Biolabs (Malvern, PA, USA). pAAV plasmid was co-transfected with Ad Helper and AAV9 rep/cap vector into HEK293 cells and, following cell harvesting, vector was purified on two CsCl gradients to obtain titre of 2.1×10^{13} GC/ml for GLDC vectors and 3.9×10^{13} GC/ml for eGFP vector.

Vector administration

For neonatal administration, mice were genotyped from tail tip sample at P0 and injected with vector or vehicle (control) into the facial vein (intra-venous; 10 µl) and/or by intra-cerebroventricular (5 µl) route at P1. At P20, intra-venous administration of vector was achieved by injection of the tail vein (10 µl).

Collection of blood and tissues

Blood was collected by terminal cardiac exsanguination, transferred to lithium-heparin tubes (BD Microtainer) and immediately centrifuged for the isolation of plasma. Tissues were rinsed in PBS and snap frozen on dry ice to store at -80 C or fixed in 10% formalin overnight.

Immunohistochemistry

For histological analysis, formalin-fixed mouse brains were dehydrated, embedded in paraffin wax and sectioned at 7 µm thickness. For immunohistochemistry, primary and secondary antibodies were anti-GFP (chicken polyclonal, 1:300; Abcam), anti-GLDC (rabbit polyclonal, 1:500; Atlas Antibodies), Alexafluor goat anti-chicken (1:250; Invitrogen) and Alexafluor goat anti-chicken (1:250, Invitrogen). For nuclear staining, cells were incubated with 4,6-diamidino-2-phenylindole (DAPI, 1:10,000 in PBS). Fluorescent images were collected on an Axiophot microscope (Zeiss) with a DC500 camera (Leica), using FireCam software (Leica).

Quantitative real time reverse transcription PCR

RNA was prepared using TRIzol reagent (Invitrogen), followed by chloroform extraction and RNA precipitation. First strand cDNA synthesis was performed using random hexamers (Superscript VILO cDNA synthesis kit). The abundance of *Gldc* mRNA was analysed by qRT–PCR (iTaq, BioRad) on BioRad CFX system, with each sample analysed in triplicate. Primers were located in exons 2 and 4 (5’ -AGCATTGATGAGCTCATCGAG-3’ and 5’ -TCCAGCAGGGAAGCGTTGGC-3’) of mouse *Gldc* and (5’-GCCCCTAGAAGCAGAGACTC-3’ and 5’-GGCACGGTTTTCTCGATCAG-3’) of human *GLDC* to amplify the wild-type but not the mutant transcript. Results were normalized to abundance of *Gapdh* expression.

Gel electrophoresis and Western blot

Brain and liver tissues were homogenised using handheld sonicator in RIPA buffer containing protease inhibitor cocktail and protein concentration in the lysate determined (Qubit). Equal total protein was loaded on NUPAGE 12% gel and protein were transferred onto PVDF membrane. GLDC protein abundance was determined using anti-GLDC antibody (Atlas antibodies), with GAPDH (detected using anti-GAPDH, Santa Cruz) as loading control. The bands were scanned using a GS800 densitometer (BioRad).

Glycine analysis

Tissue extracts were prepared by sonication in PBS containing 1x protease inhibitor cocktail (Roche). An aliquot was removed for protein determination by the Qubit assay. Tissue debris were removed by centrifugation (12,000 g at 4 C). Plasma and tissue lysate glycine were measured following the Kairos amino acid sample preparation and method (Waters corporation, UK). Briefly, protein was removed by the addition of 5-sulphosalicylic acid containing a specified quantity of amino acid internal standard in a ratio of 1:1 (sample:internal standard solution). Samples were derivatised using AccQ.Tag reagent. Glycine was resolved and detected using CORTECS UPLC C18, 1.6 µm, 2.1 x 150 mm column on an UPLC coupled to XEVO-TQS mass spectrometer (Waters Corporation, UK). Betaine and choline were analysed by LC-MS/MS (Metabolon Ltd, USA).

Folate analysis

Tissue extracts were prepared by homogenization of samples by sonication in buffer containing 20 mM ammonia acetate, 0.1% ascorbic acid, 0.1% citric acid and 100 mM dithiothreitol at pH 7. An aliquot was removed for protein determination by the Qubit assay. Proteins were then precipitated using by addition of two volumes of acetonitrile followed by centrifugation (12,000 g at 4°C). Supernatants were transferred, lyophilized, stored at -80°C and re-suspended in dH2O before analysis. Folate analysis was carried out by ultra performance liquid chromatography tandem mass spectrometry (UPLC-MS/MS) as described previously [36,44]. Lyophilized samples were resuspended in 30 l water (milli-Q) and centrifuged for 5 min at 12,000 g at 4 C. Metabolites were resolved by reversed-phase UPLC (Acquity UPLC BEH C18 column, Waters Corporation, UK). Solvents for UPLC were as follows: Buffer A, 5% methanol, 95% Milli-Q water and 5 mM dimethylhexylamine at pH 8.0; Buffer B, 100% methanol, 5 mM dimethylhexylamine. The column was equilibrated with 95% Buffer A: 5% Buffer B. The sample injection volume was 25 µl. The UPLC protocol consisted of 95% Buffer A: 5% Buffer B for 1 min, followed by a gradient of 5–60% Buffer B over 9 min and then 100% Buffer B for 6 min before re-equilibration for 4 min. The metabolites were eluted at a flow rate of 500 nl/min and the wash step with 100% Buffer B was at flow rate of 600 nl/min. The UPLC was coupled to a XEVO-TQS mass spectrometer (Waters Corporation) operating in negative-ion mode using the following settings: capillary 2.5 kV, source temperature 150 C, desolvation temperature 600 C, cone gas flow rate 150 l/h , and desolvation gas flow rate

1,200 l/h. Folates were measured by multiple reaction monitoring with optimized cone voltage and collision energy for precursor and product ions [36,45].

Statistical Analysis

Pairwise comparisons were made by t-test. Multiple groups were compared by ANOVA with post-hoc analysis by Holm-Sidak method.

Acknowledgments

This study was funded by LifeArc, Joseph's Goal and Action Medical Research (GN2403). We are also grateful for support from the Mikaere Foundation and Miichen e.V. The authors thank Rajvinder Karda, Joanna Davidge, Stephanie Schorge, Paul Gissen, John Counsell and Julian Baruteau for helpful discussions. Mass spectrometry was supported by the GOS ICH Biological Mass Spectrometry Facility. Research infrastructure at UCL GOS Institute Research was supported by the National Institute for Health Research Biomedical Research Centre at Great Ormond Street Hospital for Children NHS Foundation Trust and University College London.

References

1. Hoover-Fong JE, Shah S, Van Hove JL, Applegarth D, Toone J, Hamosh A. Natural history of nonketotic hyperglycinemia in 65 patients. *Neurology* 2004;**63**:1847-1853.

2. Kikuchi G, Motokawa Y, Yoshida T, Hiraga K. Glycine cleavage system: reaction mechanism, physiological significance, and hyperglycinemia. *Proc Jpn Acad Ser B Phys Biol Sci* 2008;**84**:246-263.

3. Hennermann JB, Berger JM, Grieben U, Scharer G, Van Hove JL. Prediction of long-term outcome in glycine encephalopathy: a clinical survey. *J Inherit Metab Dis* 2012;**35**:253-261.

4. Hennermann JB. Nonketotic hyperglycinemia and epilepsy. *Journal of Pediatric Epilepsy* 2014;**3**:207-215.

5. Swanson MA, Coughlin CR, Jr., et al. Biochemical and molecular predictors for prognosis in nonketotic hyperglycinemia. *Ann Neurol* 2015;**78**:606-618.

6. Coughlin CR, Swanson MA, et al. The genetic basis of classic nonketotic hyperglycinemia due to mutations in GLDC and AMT. *Genet Med* 2017;**19**:104-111.

7. Johnson MT, Yang HS, Magnuson T, Patel MS. Targeted disruption of the murine dihydrolipoamide dehydrogenase gene (*Dld*) results in perigastrulation lethality. *Proc Natl Acad Sci USA* 1997;**94**:14512-14517.

8. Leung KY. Glycine Cleavage System H Protein is essential for embryonic viability, implying additional function beyond the glycine cleavage system. . *Frontiers in Genetics* 2021;**12**:625120.

9. Kure S, Kato K, et al. Comprehensive mutation analysis of GLDC, AMT, and GCSH in nonketotic hyperglycinemia. *Hum Mutat* 2006;**27**:343-352.

10. Arribas-Carreira L, Dallabona C, et al. Pathogenic variants in GCSH encoding the moonlighting H-protein cause combined nonketotic hyperglycinemia and lipoate deficiency. *Hum Mol Genet* 2023;**32**:917-933.

11. Mayr JA, Zimmermann FA, Fauth C, Bergheim C, Meierhofer D, Radmayr D, Zschocke J, Koch J, Sperl W. Lipoic acid synthetase deficiency causes neonatal-onset epilepsy, defective mitochondrial energy metabolism, and glycine elevation. *Am J Hum Genet* 2011;**89**:792-797.

12. Baker PR, 2nd, Friederich MW, et al. Variant non ketotic hyperglycinemia is caused by mutations in LIAS, BOLA3 and the novel gene GLRX5. *Brain* 2014;**137**:366-379.

13. Dinopoulos A, Kure S, Chuck G, Sato K, Gilbert DL, Matsubara Y, Degrauw T. Glycine decarboxylase mutations: a distinctive phenotype of nonketotic hyperglycinemia in adults. *Neurology* 2005;**64**:1255-1257.

14. Dinopoulos A, Matsubara Y, Kure S. Atypical variants of nonketotic hyperglycinemia. *Mol Genet Metab* 2005;**86**:61-69.

15. Brunel-Guitton C, Casey B, Coulter-Mackie M, Vallance H, Hewes D, Stockler-Ipsiroglu S, Mercimek-Mahmutoglu S. Late-onset nonketotic hyperglycinemia caused by a novel homozygous missense mutation in the GLDC gene. *Mol Genet Metab* 2011;**103**:193-196.

16. Baumgartner R, Ando T, Nyhan WL. Nonketotic hyperglycinemia. *J Pediatr* 1969;**75**:1022-1030.

17. Van Hove JL, Vande KK, Hennermann JB, Mahieu V, Declercq P, Mertens S, De BM, Kishnani PS, Jaeken J. Benzoate treatment and the glycine index in nonketotic hyperglycinaemia. *J Inherit Metab Dis* 2005;**28**:651-663.

18. Van Hove JL, Kishnani P, Muenzer J, Wenstrup RJ, Summar ML, Brummond MR, Lachiewicz AM, Millington DS, Kahler SG. Benzoate therapy and carnitine deficiency in non-ketotic hyperglycinemia. *Am J Med Genet* 1995;**59**:444-453.

19. Hamosh A, Maher JF, Bellus GA, Rasmussen SA, Johnston MV. Long-term use of high-dose benzoate and dextromethorphan for the treatment of nonketotic hyperglycinemia. *J Pediatr* 1998;**132**:709-713.

20. Bjoraker KJ, Swanson MA, et al. Neurodevelopmental Outcome and Treatment Efficacy of Benzoate and Dextromethorphan in Siblings with Attenuated Nonketotic Hyperglycinemia. *J Pediatr* 2016;**170**:234-239.

21. Shchelochkov OA, Dickinson K, Scharschmidt BF, Lee B, Marino M, Le MC. Barriers to drug adherence in the treatment of urea cycle disorders: Assessment of patient, caregiver and provider perspectives. *Mol Genet Metab Rep* 2016;**8**:43-47.

22. Issa SS, Shaimardanova AA, Solovyeva VV, Rizvanov AA. Various AAV Serotypes and Their Applications in Gene Therapy: An Overview. *Cells* 2023;**12**.

23. Sehara Y, Fujimoto KI, Ikeguchi K, Katakai Y, Ono F, Takino N, Ito M, Ozawa K, Muramatsu SI. Persistent Expression of Dopamine-Synthesizing Enzymes 15 Years After Gene Transfer in a Primate Model of Parkinson's Disease. *Hum Gene Ther Clin Dev* 2017;**28**:74-79.

24. Foust KD, Nurre E, Montgomery CL, Hernandez A, Chan CM, Kaspar BK. Intravascular AAV9 preferentially targets neonatal neurons and adult astrocytes. *Nat Biotechnol* 2009;**27**:59-65.

25. Foust KD, Salazar DL, et al. Therapeutic AAV9-mediated suppression of mutant SOD1 slows disease progression and extends survival in models of inherited ALS. *Mol Ther* 2013;**21**:2148-2159.

26. Xie C, Gong XM, Luo J, Li BL, Song BL. AAV9-NPC1 significantly ameliorates Purkinje cell death and behavioral abnormalities in mouse NPC disease. *J Lipid Res* 2017;**58**:512-518.

27. Hughes MP, Smith DA, et al. AAV9 intracerebroventricular gene therapy improves lifespan, locomotor function and pathology in a mouse model of Niemann-Pick type C1 disease. *Hum Mol Genet* 2018;**27**:3079-3098.

28. Pan X, Sands SA, Yue Y, Zhang K, LeVine SM, Duan D. An Engineered Galactosylceramidase Construct Improves AAV Gene Therapy for Krabbe Disease in Twitcher Mice. *Hum Gene Ther* 2019;**30**:1039-1051.

29. Bravo-Hernandez M, Tadokoro T, et al. Spinal subpial delivery of AAV9 enables widespread gene silencing and blocks motoneuron degeneration in ALS. *Nat Med* 2020;**26**:118-130.

30. Hughes MP, Nelvagal HR, Coombe-Tennant O, Smith D, Smith C, Massaro G, Poupon-Bejuit L, Platt FM, Rahim AA. A Novel Small NPC1 Promoter Enhances AAV-Mediated Gene Therapy in Mouse Models of Niemann-Pick Type C1 Disease. *Cells* 2023;**12**.

31. Meyer K, Ferraiuolo L, et al. Improving single injection CSF delivery of AAV9-mediated gene therapy for SMA: a dose-response study in mice and nonhuman primates. *Mol Ther* 2015;**23**:477-487.

32. Pattali R, Mou Y, Li XJ. AAV9 Vector: a Novel modality in gene therapy for spinal muscular atrophy. *Gene Ther* 2019;**26**:287-295.

33. Kuzmin DA, Shutova MV, Johnston NR, Smith OP, Fedorin VV, Kukushkin YS, van der Loo JCM, Johnstone EC. The clinical landscape for AAV gene therapies. *Nat Rev Drug Discov* 2021;**20**:173-174.

34. Pai YJ, Leung KY, Savery D, Hutchin T, Prunty H, Heales S, Brosnan ME, Brosnan JT, Copp AJ, Greene ND. Glycine decarboxylase deficiency causes neural tube defects and features of non-ketotic hyperglycinemia in mice. *Nat Commun* 2015;**6**:6388.

35. Leung KY, De Castro SCP, Santos C, Savery D, Prunty H, Gold-Diaz D, Bennett S, Heales S, Copp AJ, Greene NDE. Regulation of glycine metabolism by the glycine cleavage system and conjugation pathway in mouse models of non-ketotic hyperglycinemia. *J Inherit Metab Dis* 2020;**43**:1186-1198.

36. Leung KY, Pai YJ, et al. Partitioning of One-Carbon Units in Folate and Methionine Metabolism Is Essential for Neural Tube Closure. *Cell Rep* 2017;**21**:1795-1808.

37. Yoshida T, Kikuchi G. Majors pathways of serine and glycine catabolism in various organs of the rat and cock. *J Biochem* 1973;**73**:1013-1022.

38. Schuster DJ, Dykstra JA, Riedl MS, Kitto KF, Belur LR, McIvor RS, Elde RP, Fairbanks CA, Vulchanova L. Biodistribution of adeno-associated virus serotype 9 (AAV9) vector after intrathecal and intravenous delivery in mouse. *Front Neuroanat* 2014;**8**:42.

39. Chakrabarty P, Rosario A, et al. Capsid serotype and timing of injection determines AAV transduction in the neonatal mice brain. *PLoS One* 2013;**8**:e67680.

40. Foust KD, Nurre E, Montgomery CL, Hernandez A, Chan CM, Kaspar BK. Intravascular AAV9 preferentially targets neonatal neurons and adult astrocytes. *Nat Biotechnol* 2009;**27**:59-65.

41. Wu Z, Yang H, Colosi P. Effect of genome size on AAV vector packaging. *Mol Ther* 2010;**18**:80-86.

42. Grieger JC, Samulski RJ. Packaging capacity of adeno-associated virus serotypes: impact of larger genomes on infectivity and postentry steps. *J Virol* 2005;**79**:9933-9944.

43. Santos C, Pai YJ, Mahmood MR, Leung KY, Savery D, Waddington SN, Copp AJ, Greene N. Impaired folate 1-carbon metabolism causes formate-preventable hydrocephalus in glycine decarboxylase-deficient mice. *J Clin Invest* 2020;**130**:1446-1452.

44. Scott TA, Quintaneiro LM, et al. Host-Microbe Co-metabolism Dictates Cancer Drug Efficacy in C. elegans. *Cell* 2017;**169**:442-456.

45. Leung KY, De Castro SC, Cabreiro F, Gustavsson P, Copp AJ, Greene ND. Folate metabolite profiling of different cell types and embryos suggests variation in folate one-carbon metabolism, including developmental changes in human embryonic brain. *Mol Cell Biochem* 2013;**378**:229-236.

Figures

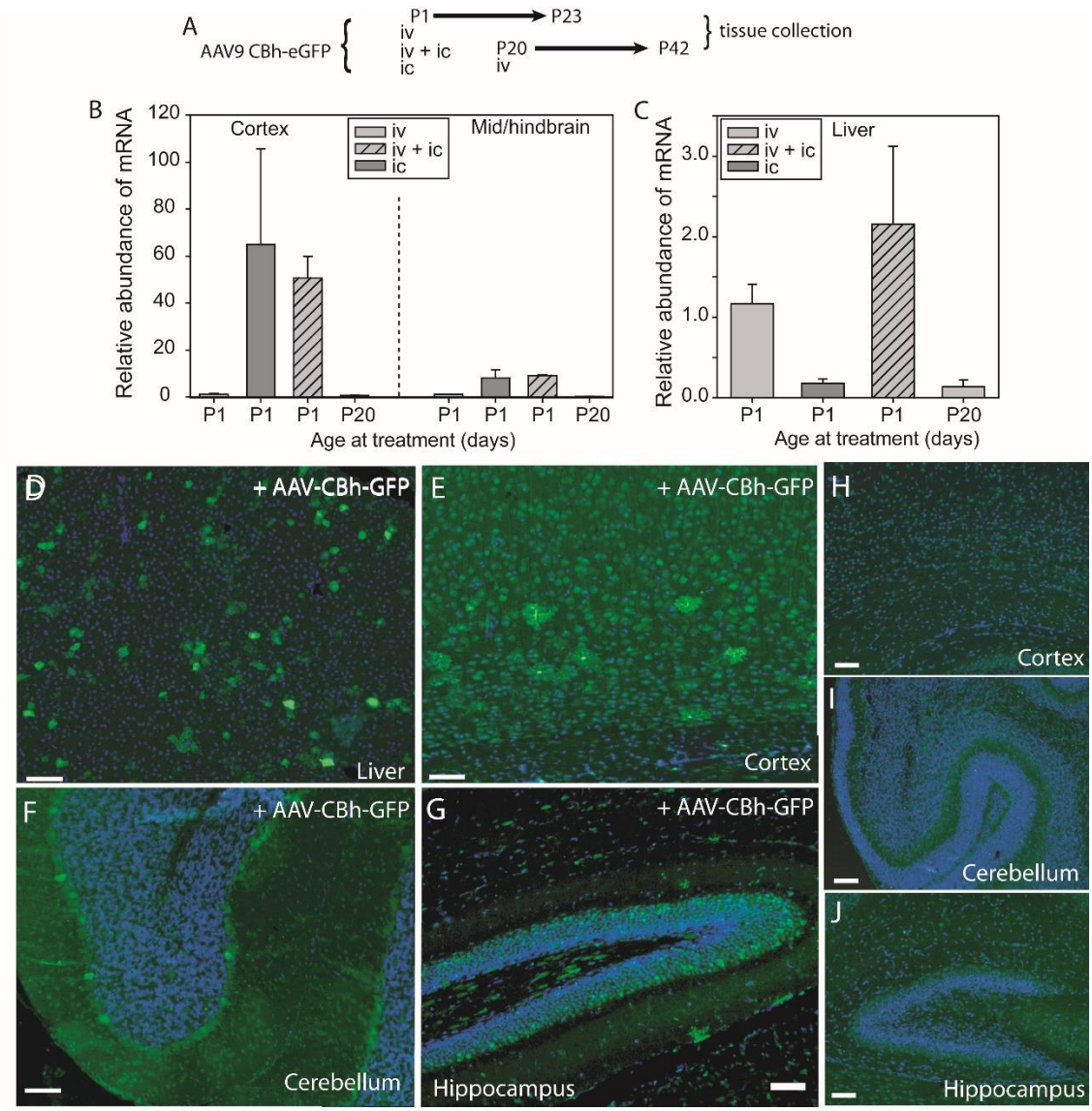

Figure 1. Evaluation of capsid and promoter combination for expression of transgene in moue brain. (A) AAV9-CBh-eGFP vector was administered to neonatal wild-type mice at post-natal day 1 (P1) ic, iv or iv and ic routes or at P20 by iv route. (B-C) Three weeks after administration of vector, *GFP* mRNA was detected in (B) brain (B) and (C) liver. (D-G) Among mice treated with AA9-CBheGFP vector, GFP protein was detected by immunostaining in (D) liver (iv or iv +ic route at P1) and (E-G) different brain regions (ic or iv +ic route) including (E) cortex, (F) cerebellum, and (G) hippocampus. Examples are from mice treated by iv + ic route. (H-J) Low level of background fluorescence in samples from untreated mice.

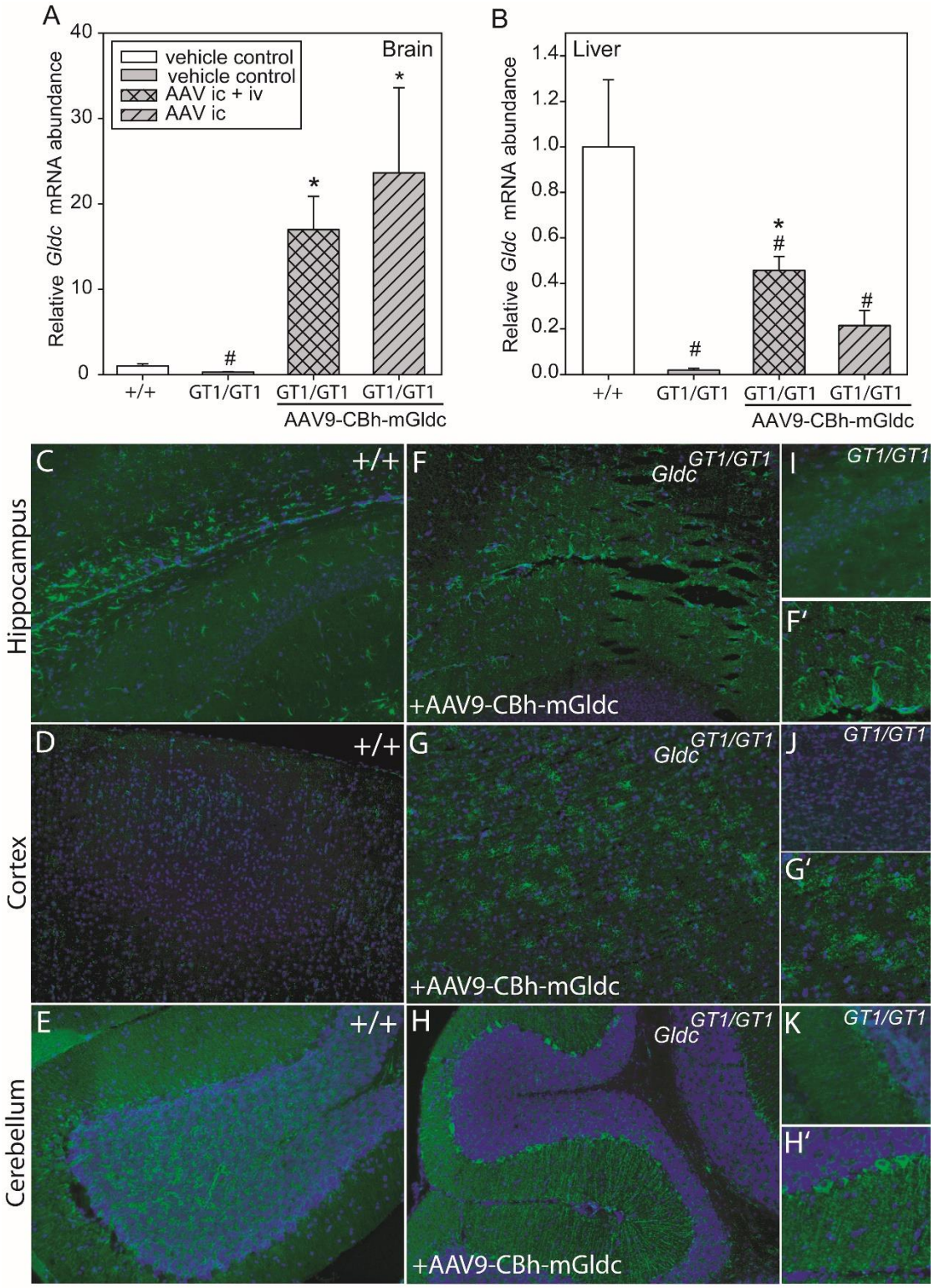

Figure 2. Expression of *Gldc* following administration of AAV vector with mouse *Gldc* to neonatal *Gldc*-deficient mice. Abundance of *Gldc* mRNA is lower in (A) brain and (B) liver of *Gldc*-deficient (*Gldc*$^{GT1/GT1}$) mice compared with wild-type (+/+) at 6 weeks of age (# significantly lower than +/+; p<0.001, t-test). (A) Administration of AAV9-CBh-mGldc led to increase in *Gldc* expression in (A) brain of *Gldc*$^{GT1/GT1}$, by either iv +ic or ic route (* significantly

different to untreated *Gldc*$^{GT1/GT1}$ or +/+, p<0.001; ANOVA), and (B) liver *Gldc*$^{GT1/GT1}$, by iv +ic route but not ic only (* significantly different to untreated *Gldc*$^{GT1/GT1}$ p<0.001; ANOVA, post-hoc analysis by Holm-Sidak method). In liver, mRNA expression in treated *Gldc*$^{GT1/GT1}$ did not reach wild-type levels at 6 weeks of age ($^{\#}$ significantly lower than +/+; p<0.001, t-test). Number of samples, n = 6 +/+, 19 *Gldc*$^{GT1/GT1}$, 9 iv + ic, 6 ic only brain samples; n = 5 +/+, 13 *Gldc*$^{GT1/GT1}$, 13 iv + ic, 13 ic only liver. (C-E) Sites of GLDC expression in brain of +/+ include (C) hippocampus, (D) cortex, and (E) cerebellum. (F-H) After ic administration of AAV9-CBh-mGLDC at P1, GLDC protein is detected in brain of *Gldc*$^{GT1/GT1}$ mice after 6 weeks, but (I-K) is not is undetectable in untreated *Gldc*$^{GT1/GT1}$ mice. (F'-H') show higher magnification images of F-H).

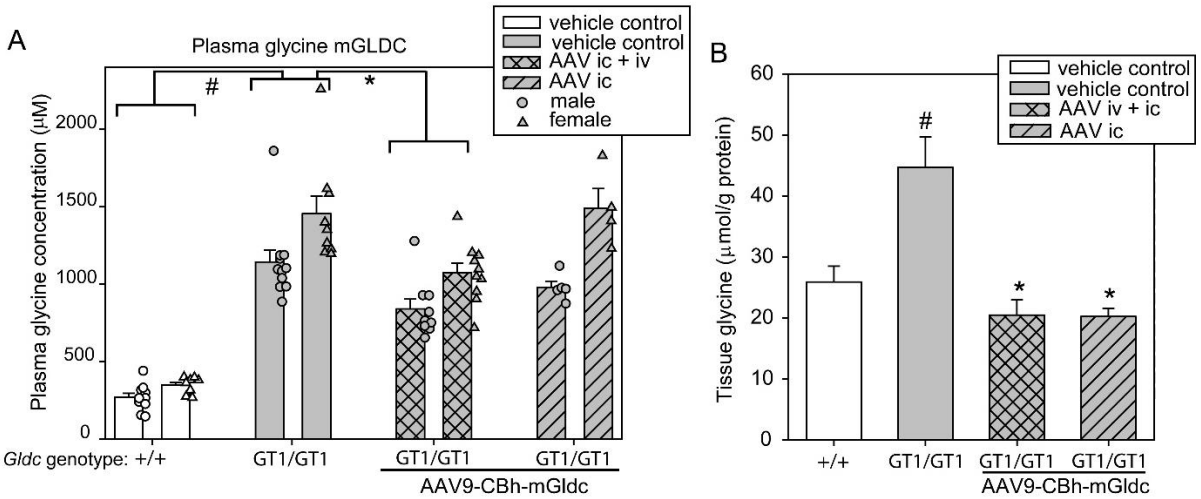

Figure 3. Administration of AAV-CBh-mGldc leads to lowering of plasma glycine.

(A) Plasma glycine is elevated in vehicle treated *Gldc*$^{GT1/GT1}$ mice compared with wild-type (+/+) littermates ($^{\#}$significantly different, p<0.001). At 6 weeks after treatment at P1 plasma glycine was lower in *Gldc*$^{GT1/GT1}$ mice treated by iv+ic route, than in vehicle treated *Gldc*$^{Gt1/GT1}$ mice (* significant difference, p<0.01). The effect of iv +ic treatment among *Gldc*$^{GtT1/GT1}$ mice was observed among male and female mice analysed separately (significant difference between mice of same sex, p<0.05). (n = 19 +/+, 21 *Gldc*$^{GT1/GT1}$, 19 *Gldc*$^{GT1/GT1}$ iv+iv treated, 9 *Gldc*$^{GT1/GT1}$ ic treated). (B) Brain tissue glycine content (normalised to protein) significantly varied between groups (p<0.001 ANOVA). Glycine was significantly elevated in *Gldc*$^{GT1/GT1}$ compared with +/+ mice ($^{\#}$p<0.01) and was significantly lowered by AAV-CBh-mGldc treatment (*p<0.02). (n = 12 +/+, 16 *Gldc*$^{GT1/GT1}$, 6 *Gldc*$^{GT1/GT1}$ iv+iv treated, 4 *Gldc*$^{GT1/GT1}$ ic treated).

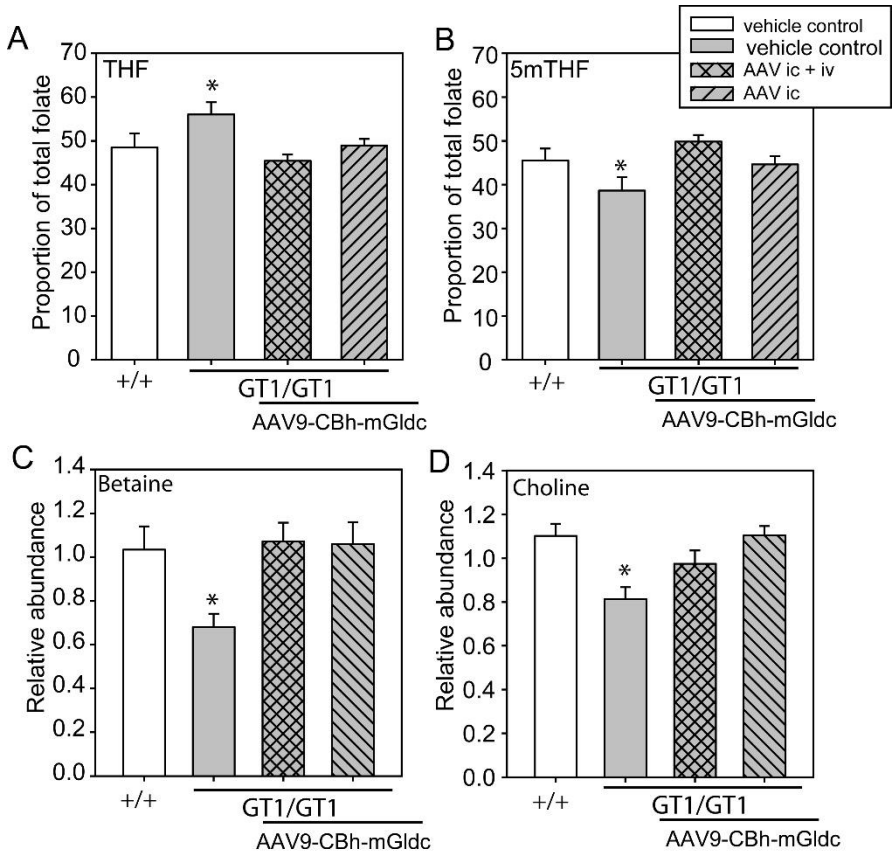

Figure 4. AAV-mediated GLDC expression normalises folate profile in brain of *Gldc*-deficient mice. (A-B) The abundance of (A) THF and (B) 5-methylTHF as a proportion of total folate differs in the brain of wild-type (+/+) and *Gldc*-deficient mice at 6 weeks of age (*significant difference between +/+ and $Gldc^{GT1/GT1}$ mice, $p<0.05$). No significant difference was observed following vector administration at P1 by iv + ic or ic routes (n = 5-6 mice per group). (C-D) Betaine and choline have significantly lower abundance in brain of *Gldc*-deficient mice than in wild-types at 6 weeks of age (*$p<0.05$; ANOVA), but abundance is normalised by administration of AAV-mGLDC by iv+ic or ic route at P1 (n = 6 mice per group).

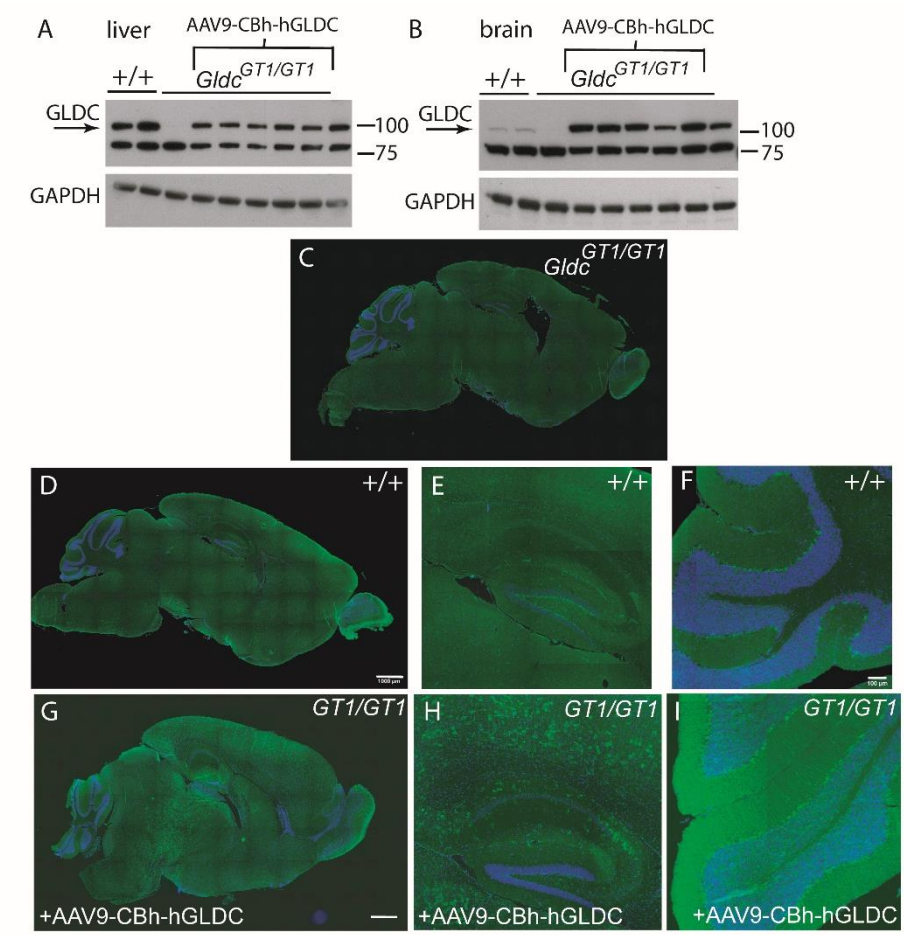

Figure 5. Expression of human GLDC protein following AAV vector administration to *Gldc*-deficient mice. (A-B) Immunoblot shows presence of endogenous mouse GLDC in (A) liver and (B) brain of wild-type (+/+) mice, but not in *Gldc*-deficient (*Gldc*$^{GT1/GT1}$) mice at 6 weeks of age. Following administration of AAV9-CBh-hGLDC vector at P1 (iv + ic route), human GLDC protein is detected in both liver and brain of *Gldc*$^{GT1/GT1}$ mice. (C—I) Immunostaining for GLDC on sagittal sections of brain at 6 weeks of aged reveals presence of GLDC protein in brain of (D-F) +/+ and (G-I) treated *Gldc*$^{GT1/GT1}$, including in hippocampus (E, H) and cerebellum (F, I), but not in untreated *Gldc*$^{GT1/GT1}$ mice (C). Whole brain images show tile scans of entire section.

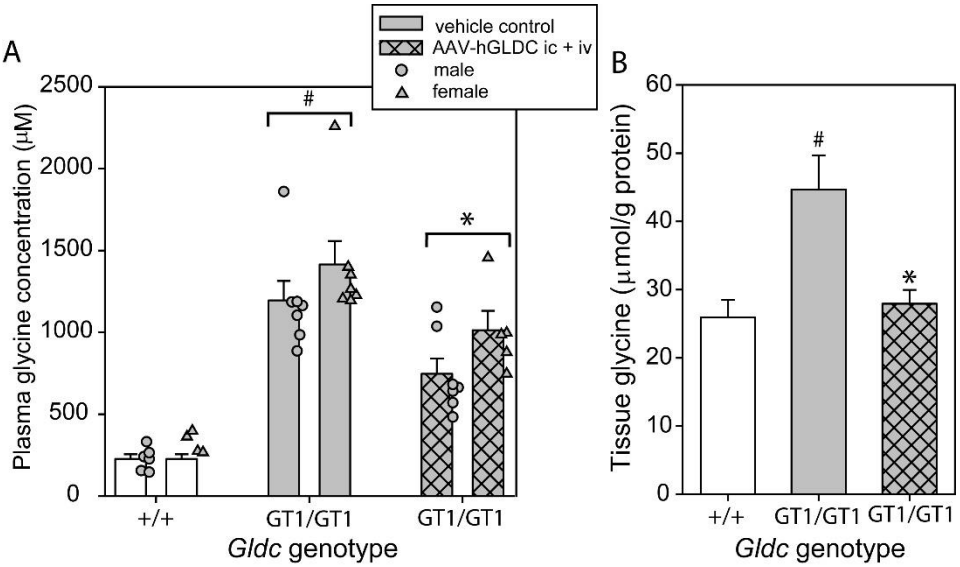

Figure 6. Lowering of plasma and brain tissue glycine by AAV vector mediated expression of human GLDC in *Gldc*-deficient mice. Plasma glycine concentration (A) and (B) brain tissue glycine (normalised to total protein content), are significantly elevated in $Gldc^{GT1/GT1}$ mice compared with +/+ at 6 weeks of age ($^{\#}$ $p<0.001$). Administration of AAV9-CBh-GLDC to neonatal mice by iv + ic route, leads to (A) significant lowering of plasma glycine compared with control $Gldc^{GT1/GT1}$ mice (* $p<0.001$ for overall group, and $p<0.05$ for individual sex comparisons), and (B) a significant reduction in brain tissue glycine abundance (* significant difference to $Gldc^{GT1/GT1}$ control group). Number of samples, n = 10-16 per group. Note that dataset for control +/+ and $Gldc^{GT1/GT1}$ overlaps with data in Figure 3 as AAV groups were treated in parallel.